Keio University

1858

CALAMVS GLADIO FORTIOR

Annual Report on Research Activities 2014

Tanabe Photonic Structure Group,

Department of Electronics and Electrical Engineering,

Faculty of Science and Technology, Keio University

Contents

Foreword

I am very thankful to everyone who is supporting our group, in the Department of Electronics and Electrical Engineering, in Keio University, Japan.

After four years, our group has grown sufficiently to regard as a research lab, since we now have a number of students and sufficient facilities that need to conduct research. Our activities are now on the stage of international conferences and journal papers; in particular, the research on photonic crystal nanocavity showed significant progress over this year.

We have selected some of our research topics, and put them together to make this report. All of the manuscripts are written by bachelors and master-course students. Therefore, I admit that some sentences are not well written. Even though, I am confident that the scientific contents provide important information and you may find interest in our research activities. I am appreciating and glad if you will give us any feedback to our researches.

August, 2015

Takasumi Tanabe, Associate Professor,
Department of Electronics and Electrical Engineering,
Keio University

Lab Members (Names and their positions after graduation)

Associate Professor

Takasumi Tanabe

Secretary

Naoko Kojima

PhD Students:

Nurul Ashikin Binti Daud

Continues her education in the graduate school of Keio University

Master 2st Grade: (The class of 2012)

Ryusuke Saito	Pursue sub-major master degree in Graduate School of Media and Governance in Keio University
Ryo Suzuki	Continues his education in the graduate school of Keio University
Tomohiro Tetsumoto	Continues his education in the graduate school of Keio University
Jiro Nishimura	Starts his carrier in industry
Akihiro Fushimi	Starts his carrier in industry

Master 1st Grade: (the class of 2013)

Tomoya Kobatake	Continues his education in the graduate school of Keio University
Sho Tamaki	Continues his education in the graduate school of Keio University
Zhelun Chen	Continues his education in the graduate school of Keio University
Yosuke Nakagawa	Continues his education in the graduate school of Keio University

Bachelor 4th Grade: (The class of 2014)

Hiroki Itobe	Continues his education in the graduate school of Keio University
Yuta Ooka	Continues his education in the graduate school of Keio University
Yusuke Okabe	Continues his education in the graduate school of Keio University
Misako Kobayashi	Continues her education in the graduate school of Keio University
Takuma Nagano	Continues his education in the graduate school of Keio University

Research Activities

Waveform Measurement of Ultra-high Repetition Mode-locked Pulses Generated from a Silica Toroid Microcavity

Zhelun Chen (M1), Ryo Suzuki (M2), Takuma Nagano (B4)

A frequency comb, which is a spectrum with broad-bandwidth modes at even intervals in the frequency domain, generates a pulse train with repetition rates of a few terahertz in the time domain. We report that we have obtained pulse trains with 6-7 terahertz repetition rates by measuring the SHG autocorrelation waveform of a Kerr comb generated from an ultra-high *Q* microcavity. Moreover, we deploy an add/drop system to obtain a higher contrast pulse train, and consider Raman scattering when generating a Kerr comb.

Keywords: frequency comb, NLO, microcavity, ultra-high repetition rates

1. Introduction

A frequency comb, which is a pencil spectrum with modes at even intervals in the frequency domain, is used as a light ruler to obtain accurate wavelength measurements. Expected applications include spectroscopy, optical clocks, GPS, and mass optical communications [1]. Frequency comb sources have included solid-state and fiber lasers. Micro-scale devices make it possible to generate a Kerr comb with lower power [2].

We studied a silica toroid microcavity [3], which has both an ultra-high Q and can be accumulated on chips. Furthermore, we determined whether or not the phases between each mode of the Kerr comb were locked by observing their autocorrelation. A mode-locked Kerr comb is expected to become the next communications light source because it can achieve ultra-high repetition rate pulse trains of over a terahertz. We report the results we obtained observing an ultra-high repetition mode-locked pulse train generated from a silica toroid microcavity.

2. Experiment method

First, we bring a toroid microcavity very close to a tapered fiber, and excitation whispering-gallery modes (WGM) through the near field. A signal from a pump laser operating at a few milliwatts and amplified by an erbium doped fiber amplifier (EDFA) through a tapered fiber is launched into the cavity above the threshold of four wave mixing (FWM) generated by a Kerr comb. When the phase of each Kerr comb mode is aligned, pulses are generated in the cavity. The Kerr comb broadened beyond the C-band in our experiments. Thus, we presume that a few hundred femtosecond, ultra-short Fourier transform limited pulses are generated. We measured the pulses in the time domain with a background-free SHG autocorrelator.

When a tapered fiber is close to the cavity, the Kerr comb generated in it passes to the output. Meanwhile, a pump laser that is not coupled with the cavity and amplified spontaneous emission (ASE) noise produced by an EDFA are also transmitted to the output. This results in output pulses with a lower contrast. Hence, we added another port, called a drop port for the second output in addition to the add port to input the pump laser into the cavity. An add/drop system poses the problem of obtaining lower contrast pulses because of input noise [4]. In this research, we attempted to measure the spectrum and pulse on the add/drop system (Figs.1, 2).

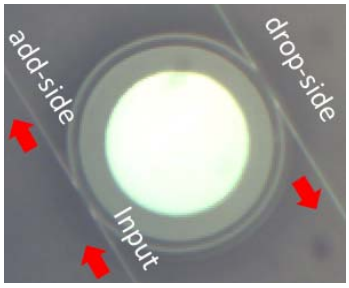

Fig.1: Photograph of add/drop system. Two fibers are coupled to a silica toroid microcavity.

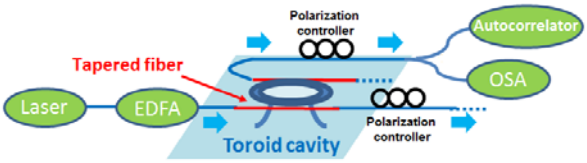

Fig. 2: Scheme of experimental setup. A laser is amplified by an erbium-doped fiber amplifier (EDFA). We measure spectra and pulses not only in the add-side but in the drop side.

3. Experimental results

First, we measured only the add port. The output from the add port was separated by a 50/50 beam splitter, then each beam was detected with an optical spectrum analyzer (OSA) and an SHG autocorrelator. The spectrum and autocorrelation waves of a Kerr comb from a microcavity are shown in Fig. 3 as an example of input laser detuning. Figure 3 (a-d) show data for the same wavelength. The vertical axis values in Fig. 3 (b) and (d) correspond to each other. The input wavelengths were (a)1546.68 nm, and (c) 1547.61 nm. The input power was 730 milliwatts. The repetition rates, f_{rep}, were (b) 6.22 THz and (d) 7.15 THz. These values correspond to the intervals between the dominant modes: (a) 7-FSR (free spectral range); (b) 8-FSR. The background of the SHG autocorrelation traces in (d) was higher than that in (b) because of the larger timing jitter of the pulses in (d). Actually, the analytics by the split-step Fourier method shows that modulational instability is apparent at a stronger input power [5]. This noise is not attributed to mode locking. Thus, the autocorrelation traces with the 1-FSR interval mode might exhibit less noise. Furthermore, Fig. 3 (a) and (c) show that there is some possibility of dominant 1-FSR interval modes induced by laser detuning in the same way. This corresponds to previously reported simulations [5, 6].

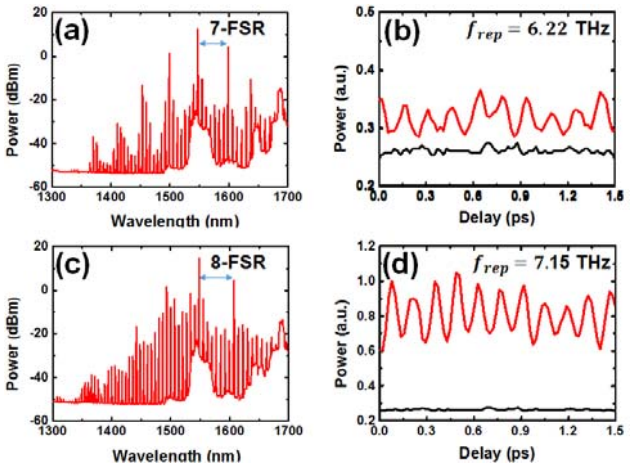

Fig. 3: Spectrum (left) and SHG autocorrelation traces (right) on the add-side.

4. Comparison ADD with DROP

The priority of an add/drop system should be discussed. Using a different cavity from the previous experiment, we compared generated Kerr combs on the add port and on the drop port. Figures 4 and 5 show the OSA spectra on the add side and on the drop side, respectively. First, it is apparent that there was no ASE noise on the drop side. Thus, while a tapered fiber was on the cavity, by accurate coupling, the ASE noise from input would not transmit to the drop port. The margin between the pump line (1549.33 nm) and the dominant comb line a distance of 8-FSR from it is over 20 dBm on the add side, meanwhile it is only 5 dBm on the drop side. This is because the pump line not coupling with the cavity propagates into the output because it is unable to be aligned with accurate critical coupling. On the other hand, because only intracavity modes couple into the output on the drop port, the flat Kerr comb is observed as seen in Fig. 4 (b).

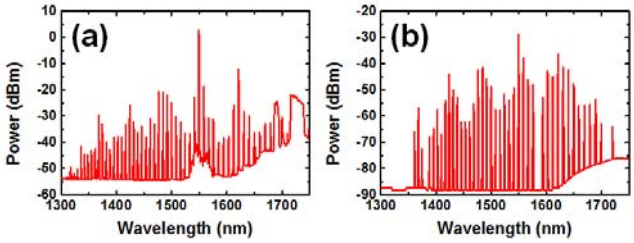

Fig. 4: Kerr comb on the ADD-port (left) and DROP-port (right).

References

[1] T. Udem, R. Holzwarth, and T. W. Hänsch, “Optical frequency metrology,” Nature **416,** 233 (2002).

[2] P. Del’Haye, A. Schliesser, O. Arcizet, T. Wilken, R. Holzwarth, and T. J. Kippenberg, “Optical frequency comb generation from a monolithic microresonator,” Nature **450**, 1214 (2007).

[3] D. K. Armani, T. J. Kippenberg, S. M. Spillane, and K. J. Vahala, “Ultra-high-Q toroid microcavity on a chip," Nature **421,** 925 (2003).

[4] P.-H. Wang, Y. Xuan, L. Fan, L. T. Varghese, J. Wang, Y. Liu, X. Xue, D. E. Leaird, M. Qi, and A. M. Weiner, “Drop-port study of microresonator frequency combs: power transfer, spectra and time-domain characterization,” Opt. Express **21,** 22441 (2013).

[5] T. Kato, T. Kobatake, R. Suzuki, Z. Chen, and T. Tanabe, “Harmonic mode locking in a high-*Q* whispering gallery mode microcavity," (arXiv: 1408.1204).

[6] T. Herr, V. Brasch, J. D. Jost, C. Y. Wang, N. M. Kondratiev, M. L. Gorodetsky, “Temporal solitons in optical microresonators,” Nat. Photonics **8,** 145 (2014).

Theoretical analysis of the influence of the thermo-optical effect on a Kerr frequency comb

Tomoya Kobatake (M1)　Takumi Kato (D1)

We generate a Kerr comb and analyze the influence on its state of the thermo-optical (TO) effect thus induced by using a theoretical analysis based on the split-step Fourier method (SSFM). We use the finite element method to obtain a parameter related to the TO effect and employ a silica toroid cavity model.

Key words: Optical frequency comb; Optical Kerr comb; Nonlinear optics; Split-step Fourier method; Thermo-optical effect;

1. Introduction

An optical frequency comb is a spectrum that consists of equidistant lines similar to a comb in the frequency domain. In the time domain, it is a repeating pulse train (Fig. 1). Optical frequency combs are called “rulers of light” because of their high accuracy and stability, and we can easily measure optical frequency by using them as a standard. Moreover, we can expect them to be applied to spectroscopy, large capacity optical communication, optical clocks, and global positioning systems (GPS) [1]. Optical frequency combs are generated using a solid-state laser (Ti:sapphire laser) or a fiber laser, and they provide highly accurate light sources. However, they are problematic in that they are large, expensive, and need a lot of energy. Therefore, the number of studies related to the Kerr comb has increased [2]. A Kerr comb has a comb-like spectrum that is realized with a small size, low cost and low energy by using the nonlinear effect in a microcavity. In particular, many theoretical studies have revealed that detuning is an important factor in relation to Kerr comb generation [3][4]. On the other hand, it is inevitable that the detuning is changed by the thermo-optic (TO) effect when we generate a Kerr comb in practice. In this study, we analyze the influence of the TO effect on a Kerr comb by using a theoretical analysis based on the split-step Fourier method (SSFM).

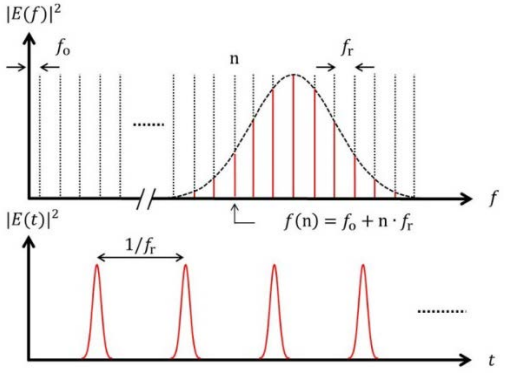

Fig. 1: Optical frequency comb in the frequency and time domains.

2. Simulation method of Kerr comb generation and introducing TO effect

A generalized mean-field Lugiato-Lefever equation (LLE) is usually used to analyze the evolution of a Kerr comb in a microcavity [3].

$$t_R \frac{\partial^2 E}{\partial r^2} = \left(-\frac{\alpha}{2} - \frac{\kappa}{2} - i\delta_0 - \frac{iL\beta_2}{2}\frac{\partial^2}{\partial t^2} + iL\gamma|E|^2 \right) E + \sqrt{\kappa} S \quad (1)$$

where, t_R, r, α, κ, δ_0, L, β_2, γ and S are the round-trip time, the number of round-trip, intrinsic cavity loss, coupling loss, the detuning of the input wavelength, cavity length, the second order dispersion of the cavity, a nonlinear coefficient, and input driving power, respectively. We can calculate the electric field in the cavity by using the SSFM.

However, we cannot consider the TO effect with (1) alone. When we consider the TO effect, the generated heat changes the cavity length and it causes a resonant wavelength shift. So we take account of the TO effect in the simulation by recalculating the detuning parameter in each step. The specific method is shown in Fig. 2. First, we normally use the SSFM to calculate the electric field in the cavity after one step. We then find the absorption loss and generated heat h from the field, and determine the heat energy U in the cavity by substituting h for the next equation.

$$\frac{dU}{dt} = -\frac{U}{\tau} + h(E^2) \quad (2)$$

$$T = U/C \quad (3)$$

where, τ is a heat lifetime, we estimate it from the simulation result with the finite element method (FEM) using a silica toroid microcavity model and the experimental result. Next, we find the temperature T of the cavity from U calculated (2) with the 4th order Runge-Kutta method and heat capacity C. Finally, we find the optical cavity length r from T, and recalculate the detuning parameter (with (4), (5)).We can take account of the TO effect in the simulation by using this detuning in the next step.

$$r = \frac{1}{n_0}(r_0 + r_0\alpha_{ex}T)\left(n_0 + \frac{dn}{dT}T\right) \quad (4)$$

$$\delta = 2\pi\left(\frac{r}{\lambda_n} - \frac{r}{\lambda}\right) \qquad (5)$$

where, r_0, α_{ex}, $\frac{dn}{dT}$ and λ_n are the optical cavity length without temperature change, the coefficient of thermal expansion, the thermos-optic coefficient and the resonant wavelength.

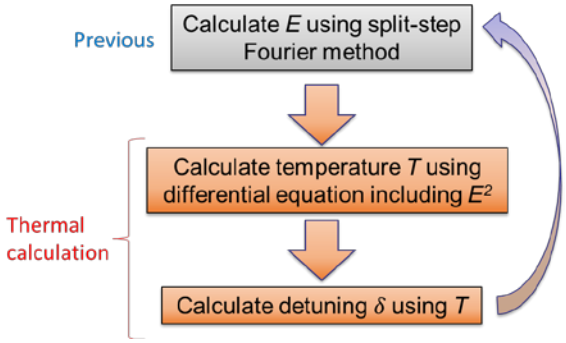

Fig. 2: The simulation method with TO effect

In this research, we mainly use the parameters of the silica toroid microcavity. We solve the LLE with the SSFM and define one step as one round-trip.

3. Simulation result

3.1 In the case when the thermo-optical coefficient is zero

First, we simulate the Kerr comb generation with $\frac{dn}{dT} = 0$, which means without the TO effect, to compare the result obtained with the TO effect and to consider its influence. The graphs at the top of Fig. 3 show the transmittance power when the input wavelength is scanned from the blue to the red wavelength. The top left shows the simulation result without the nonlinear effect and it forms a normal resonant spectrum. On the other hand, the transmission spectrum can be roughly divided into three regions as shown in the top right of Fig. 3 when the input power is high enough for the nonlinear optical effect to occur. From the shortest wavelength, the regions are ① modulated state, ② unstable state and ③ soliton state. Each timescale waveform is shown at the bottom of Fig. 3.

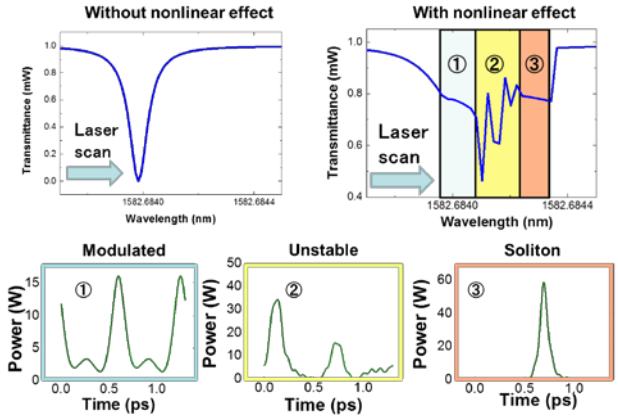

Fig. 3: Transmittance spectrum when the thermo-optical coefficient is zero, without (top left) and with (top right) nonlinear effect. The bottom shows the timescale waveforms in the three regions shown in the top right.

3.3 Positive thermo-optical coefficient

Silica is a material that we assume has a positive thermo-optical coefficient. In this case, the simulation result for the transmittance power is shown in Fig. 4 (left) when we scan the input from short to long wavelengths. The scan is realized by changing the detuning parameter after calculating enough steps with constant detuning. From this result, we can see that the transmittance spectrum becomes triangular because of the resonant wavelength shift caused by the TO effect. In addition, there are only regions ① and ②, and it has become off resonance before ③. The reason for this can be expected from Fig. 4 (right), which shows the temporal change in the power and temperature in the cavity when it is out of resonance. In this figure, it temporarily enters the soliton state, but finally becomes out of resonance because the power in the cavity decreases from state ② to state ③, and the temperature continues to decrease. Therefore, to obtain a soliton, we need to scan the input wavelength at an appropriate speed so as not to change the temperature very much during the transition from ②to ③ [5].

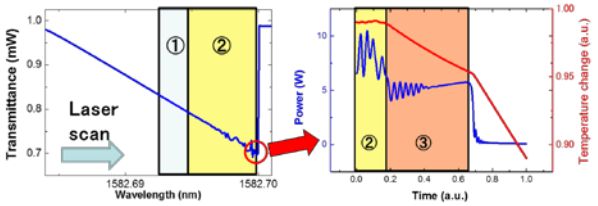

Fig. 4: Transmittance spectrum when the thermo-optical coefficient is positive (left). The temporal change in the temperature and the power in the cavity at the wavelength when it is out of resonance (right).

3.3 Negative thermo-optical coefficient

We investigated the case when the thermo-optical coefficient was negative. For example, it is known that a cavity made of CaF_2 has a negative thermo-optical coefficient. In this study, for the sake of simplicity, we used the parameters of the silica toroid cavity except for the inverse thermo-optical coefficient. We also assume that there is always thermal equilibrium. Figure 5 shows the transmittance power. The input wavelength was scanned from red to blue because a negative thermo-optical coefficient makes the wavelength shift in that direction. We can see that only region ③has a negative thermo-optical coefficient. This results from the fact that the shifts induced by the Kerr and TO effects are in opposite directions. First, the modulation by Kerr effect increases the power in the cavity and this further increases the Kerr effect. After that, it remains in the soliton region because of the equilibrium between the TO and

Kerr effects.

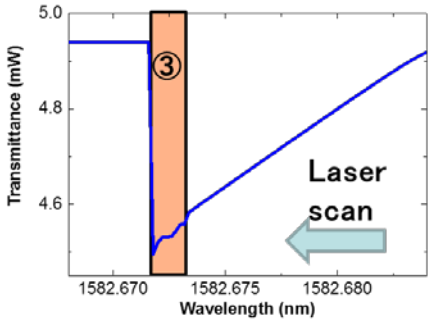

Fig. 5: Transmittance spectrum when the thermo-optical coefficient is negative.

4. Conclusion

We took account of the TO effect in a simulation with the SSFM by considering the detuning parameter to be a function of the power in the cavity. We investigated the influence of the TO effect on Kerr comb generation. It is difficult to maintain a soliton state with a positive thermo-optic coefficient. On the other hand, it automatically realizes a soliton state with a negative thermo-optical coefficient because the Kerr and TO effects cause the wavelength to shift in opposite directions.

References

[1] T. Udem, R. Holzwarth, and T. W. Hansch, Nature **416**, 233-237 (2002).
[2] P. Del'Haye, A. Schliesser, O. Arcizet, T. Wilken, R. Holzwarth, and T. J. Kippenberg, Nature **450**, 1214-1217 (2007).
[3] S. Coen, H. Randle, T. Sylvestre, and M. Erkintalo, Opt. Lett. **38,** 37 (2013).
[4] C. Godey, I. Balakireva, A. Coillet, and Y. Chembo, Phys. Rev. A **89**, 063814(2014)
[5] T. Herr, V. Brash, J. Jost, C. Wang, N. Kondratiev, M. Gorodetsky, and T. Kippenberg, Nature Photon. **8**, 145-152 (2014)

Establishment of factor technique for stabilization of Kerr comb

Yusuke Okabe (B4)　Tomoya Kobatake (M1)　Zhelun Chen (M1)

A Kerr comb created with a high-Q microcavity is similar to an optical frequency comb (OFC). It can be made more cheaply and more compact than an OFC, and so OFC devices may be made smaller by replacing the OFC with a Kerr comb. However, a Kerr comb has insufficient stability. In this research, to obtain a more stable Kerr comb, we control the pump laser frequency and power, and furthermore we reduce the mechanical oscillation noise.

Keyword : optical frequency comb, microcomb, nonlinear optics, toroidal microcavity, feedback control, cavity opto-mechanics

1. Background

A Kerr comb is created by cascading spectra generated with a 3rd order nonlinear optical effect in a microcavity. The spectra occupy the same space because of the law of energy conservation. A Kerr comb can be made more cheaply and more compactly than an OFC, and so OFC devices may become smaller if we replace the OFC with a Kerr comb. However, a Kerr comb has insufficient stability to apply it to practical devices. In this research, to increase the stability of the Kerr comb, we control the pump laser frequency and power, and furthermore we reduce the mechanical oscillation noise.

2. Fluctuation and noise of Kerr comb

The fluctuation of a Kerr comb (= fluctuation of mode spacing) is caused partly by the pump frequency and pump power[1]. The pump power affects the temperature of the microcavity by changing the amount of absorbed light and then the mode spacing is modified due to the change of the refractive index. The pump frequency also affects the pump power since modifying the detuning of the cavity resonance means altering the coupling level, which in practice means changing the pump power (Fig. 1). That is, the two factors related to pump light control affect the stabilization of the mode spacing of the Kerr comb.

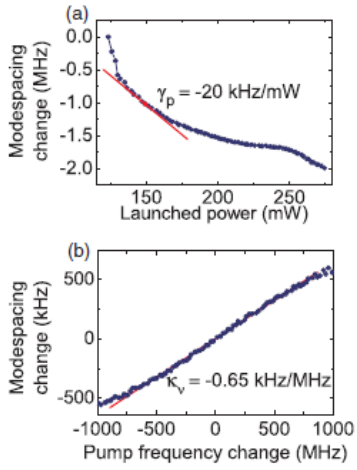

Fig. 1. (a) Dependence of mode spacing on power launched into microcavity. (b) Dependence of mode spacing on pump laser frequency. [P. Del'Haye *et al.*, "Full stabilization of a microresonator-based optical frequency comb," Phys. Rev. Lett. **101**, 053903 (2008).]

The noise of a Kerr comb is partly caused by mechanical oscillation, which is one feature of cavity opto-mechanics. The noise arises when the pump light is launched into a microcavity with sufficient power[2]. Chaotic oscillation occurs when the pump power increases[3] and it modifies the power of the Kerr comb. Therefore, this vibration must be reduced.

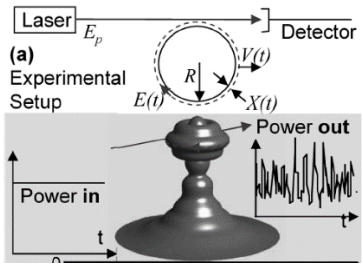

Fig. 2. Schematic model of cavity opto-mechanics. [T. Carmon, *et al.*, "Chaotic quivering of micron-scaled on-chip resonators excited by centrifugal optical pressure," Phys. Rev. Lett. 98, 167203 (2007).]

3. Feedback control of pump power and frequency

We employ proportional-integral-derivative (PID) control to stabilize the pump power and frequency.

First, we show the experimental setup for PID control of the pump power in Fig. 3.

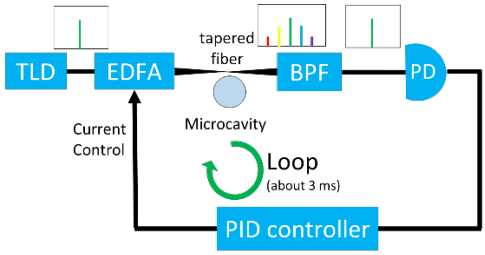

Fig. 3. Experimental setup for PID control of pump power (TLD: Tunable laser diode, EDFA: Erbium doped optical fiber amplifier, BPF: Band pass filter, PD: Photodiode)

Pump light amplified by an EDFA was launched into the microcavity and generated a Kerr comb. Then the pump light cut by a band-pass filter was converted to current with a photodiode. The PID controller received the current and stabilized it by modifying the current of the EDFA (= amplification factor). The current receiver and controller, respectively, were NI-9215 and NI-9263 made by National Instruments, and the PID algorithm was run with a PC. Fig. 4 shows the result.

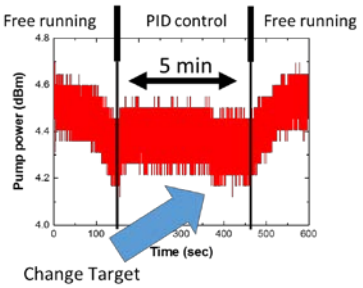

Fig. 4. Result of PID control of pump power

This shows that we can control the pump power for more than 5 minutes. The arrow indicates that the controller followed when we changed the target power. The voltage resolution of NI-9263 is only 0.3 mV because of quantization error.

Next, we show the experimental setup for the PID control of pump frequency in Fig. 5.

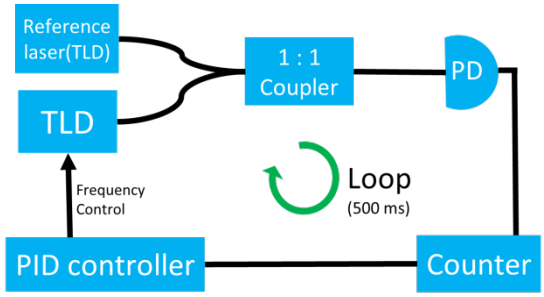

Fig. 5. Experimental setup of PID control of pump frequency (TLD: Tunable laser diode, PD: Photodiode, Counter: Frequency counter.)

The beat of the pump laser and reference laser was converted to current with a photodiode. The PID controller received the frequency from a frequency counter and modified the pump frequency to stabilize the beat frequency. Fig. 6 shows the result.

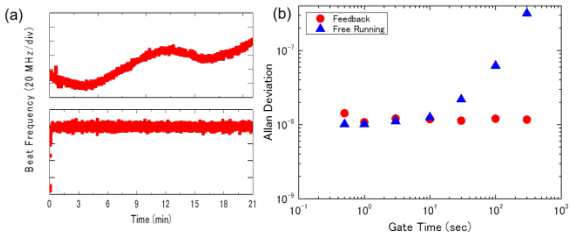

Fig. 6. (a) Beat frequency. The figures show free-running and under PID control, respectively. The target frequency was 200 MHz. (b) Allan deviation of free-running (blue triangle) and stabilized pump laser (red circle).

The Allan deviation of the stabilized laser is 1×10^{-8} at 100s in contrast to that of a free-running laser, which is 6×10^{-8}.

4. Reduction of mechanical oscillation

We reduced the mechanical oscillation of the Kerr comb by changing the detuning of the cavity resonance. This mechanism is called cavity opto-mechanics, which is analogous to atom cooling, and it is known that the vibration is reduced by blue detuning. We applied this method to the Kerr comb. Fig. 7 shows the result.

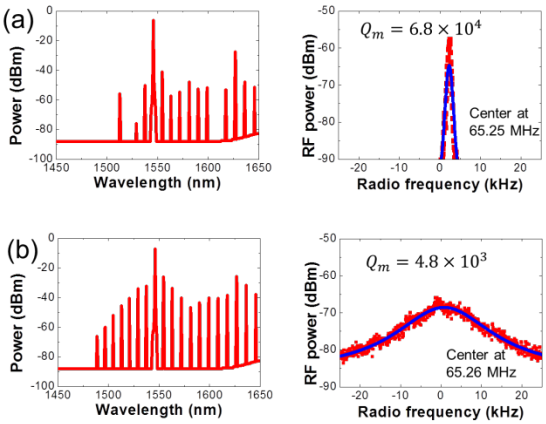

Fig. 7. (a) Kerr comb and RF noise spectra at a pump wavelength of 1545.300 nm. This RF noise was about -60 dBm and the mechanical Q-factor was 6.8×10^4. (b) Kerr comb and RF noise spectra obtained by increasing the wavelength by 34 pm (= pump wavelength 1545.334 nm). This RF noise was about -70 dBm and the mechanical Q-factor was 4.8×10^3.

We reduced the RF noise by about 10 dB and the mechanical Q-factor by more than one digit.

5. Conclusion

We controlled the pump laser power and frequency by using a feedback controller for Kerr comb stabilization, and we reduced the mechanical oscillation of the Kerr comb by changing the detuning of the cavity resonance to a low frequency. We may be able to obtain a stabilized Kerr comb by combining these techniques.

Reference

[1] P. Del'Haye, O. Arcizet, A. Schliesser, R. Holzwarth, and T. Kippenberg, "Full stabilization of a microresonator-based optical frequency comb," Phys. Rev. Lett. **101**, 053903 (2008).

[2] H. Rokhsari, T. Kippenberg, T. Carmon, and K. Vahala, "Radiation-pressure-driven micro-mechanical oscillator," Opt. Express **13**, 5293 (2005).

[3] T. Carmon, M. Cross, and K. Vahala, "Chaotic quivering of micron-scaled on-chip resonators excited by centrifugal optical pressure," Phys. Rev. Lett. **98**, 167203 (2007).

Integration of silica toroid microcavity and tapered optical fiber

Misako Kobayashi (B4)　Jiro Nishimura (M2)

To conduct an experiment using a silica toroid microcavity, it is necessary to control precisely the positional relationship between the microcavity and a tapered optical fiber. However, this requires a highly accurate moving stage, and there is a problem in that a silica toroid microcavity cannot be applied in a large field. In this research, we attempted to integrate a silica toroid microcavity and a tapered optical fiber in a measurable state.

Key words: Silica toroid microcavity; Tapered optical fiber; Packaging

1. Introduction

An optical microcavity is a device that can strongly confine light and store it in a micro space for long periods. In recent years, the silica toroid microcavity, which is a whispering gallery mode (WGM) cavity, has attracted considerable attention [1]. The advantages of the silica toroid microcavity are that it has an ultra-high Q factor, it can be made of a single material (Si-SiO_2), and it is suitable for integration.

The silica toroid microcavity has many potential applications, e.g. optical comb generation and ultra-high sensitivity sensing [2]. Because the excitation of a resonance mode with a tapered optical fiber is necessary when performing a measurement, precise control is required of the positional relationship between the silica toroid microcavity and tapered optical fiber. As a result, the integration and packaging of a WGM cavity and tapered optical fiber has attracted attention in recent years. It has been studied by Y. Yan, *et al.* [3], F. Monifi *et al.* [4] and others, but the method they used is unsuitable for optical comb generation and ultra-high sensitivity sensing because UV curable polymer is attached to the WGM cavity.

In this research, we developed a packaging method where the UV curable polymer is not directly attached to the silica toroid microcavity.

2. Consideration of packaging method

As previously noted, the present packaging method has limited applications because UV curable polymer is attached to the WGM cavity. In addition, the current method uses UV curable polymer, which has a low refractive index of about 1.3 and low hardness, and a packaged cavity made with this method is considered to have low stability. Therefore, we used a UV curable polymer with a high refractive index of about 1.6 and high hardness and packaged the silica toroid microcavity and tapered optical fiber using the procedure shown in Fig. 1.

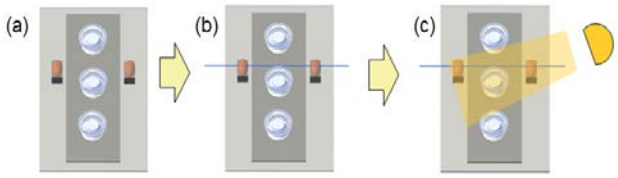

Fig 1：Experimental procedure for packaging a silica toroid microcavity and tapered optical fiber. (a) Put UV curable polymer on silicon chips. (b) Align tapered optical fiber and silica toroid microcavity. (c) Employ UV exposure for about 30 min.

Furthermore, we fabricated and used silica toroid microcavities with stands as shown in Fig. 2 to enhance the strength of the packaged cavity.

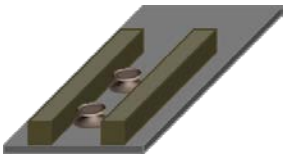

Fig 2：Silica toroid microcavity with stands.

3. Assessment of packed cavity

A packaged cavity made with the abovementioned procedure is shown in Fig. 3. Transmittance spectra obtained before and after UV light exposure and after the removal of the fiber holder are shown in Fig. 4. As shown in Figs. 3 and 4, we found that a silica toroid microcavity and a tapered optical fiber can be packaged in a small portable box, and the Q of the packaged cavity was 1.7×10^6.

Because we align the silica toroid microcavity and tapered fiber taking account of the shrinkage of the UV curable polymer caused by UV light exposure, in Fig. 4 resonance only occurs after UV light exposure. In addition, there are many resonance modes in the transmittance spectrum after UV light exposure and the removal of the fiber holder because it is thought that the silica toroid microcavity comes into contact with the tapered optical fiber. In fact, Fig. 3 shows that the tapered optical fiber touches the silica toroid microcavity.

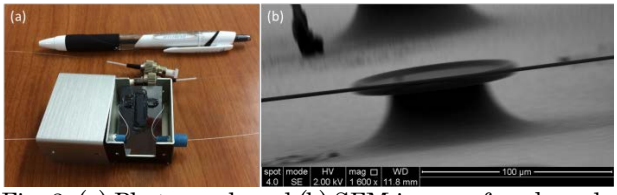

Fig. 3: (a) Photograph and (b) SEM image of packaged cavity.

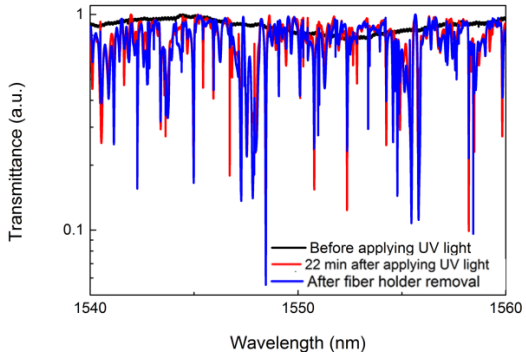

Fig. 4: Transmittance spectra obtained before UV light exposure, after UV light exposure and after fiber holder removal.

Additionally, we assessed the stability of the packaged cavity from two standpoints, the elapsed time after fabrication and the effect of vibration beginning with the former.

Transmittance spectra obtained soon, 3 days and 14 days after fabrication are shown in Fig. 5 and the change in Q is shown in Tab. 1. From Fig. 5 and Tab. 1, it is clear that the Q value of the packaged cavity decreases but resonance occurs. The cause of the decrease in the Q of packaged cavity is that dust and OH^- radicals become attached to the silica toroid microcavity and the intrinsic Q of the packaged cavity is reduced.

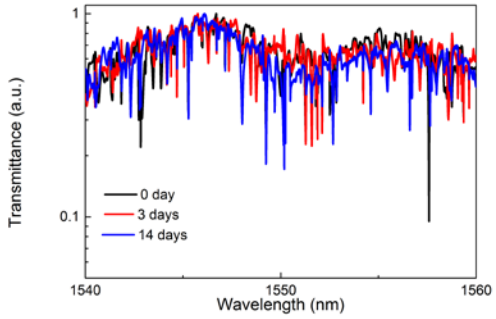

Fig. 5: Transmittance spectra soon, 3 days and 14 days after fabrication.

Tab. 1: Change in Q factor soon, 3 days and 14 days after fabrication.

Days elapsed	Q factor
0 days	1.7×10^6
3 days	6.7×10^5
14 days	4.6×10^5

Next, we studied the vibration tolerance by using a method where we approximated an ultrasonic speaker of 40 kHz to silica toroid microcavity and tapered optical fiber on resonance. The results are shown in Fig. 6. From Fig. 6, as a result of packaging swing of fiber is approximately 0 when vibration does not exist, and swing of fiber lightens up when even vibration exists. Therefore, it is apparent to lighten up the swing of fiber resulted from environmental vibration by packaging.

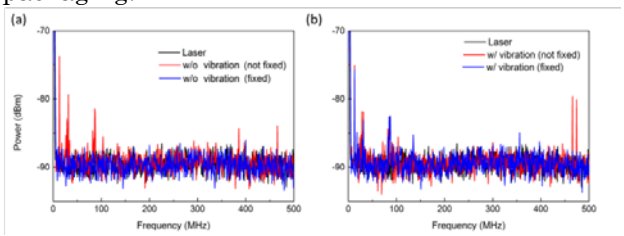

Fig. 6: Comparison of swing of fiber for packaged and unpackaged cavity (a) without vibration (b) with vibration.

4. Packaging in microfluidic channel toward sensing

As previously noted, it is possible to perform ultra-high sensitivity sensing with a silica toroid microcavity. However, there are few precedents for the development of small portable sensor. In this section, we describe how we attempted to fabricate a small portable sensor by packaging it in a microfluidic channel that we made using the packaging method reported in this study.

A cavity packaged in a microfluidic channel is shown in Fig. 7. Figure 8 shows the result of a measurement performed in a liquid environment. As shown in Fig. 8, resonance occurs even when pure water flows into the microfluidic channel, and it should be noted that we can package the silica toroid microcavity and tapered optical fiber in a measurable state not only in air but also in water. The cavity packaged in a microfluidic channel has $Q = 1.7\times10^6$ in air and $Q = 1.6\times10^4$ in water. However, there is a problem that remains to be solved, namely that the extraction rate is currently low. We will also study sensing by using a cavity packaged in a microfluidic channel.

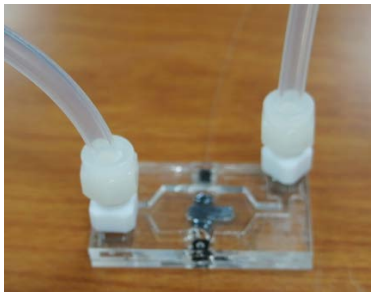
Fig. 7: Cavity packaged in microfluidic channel.

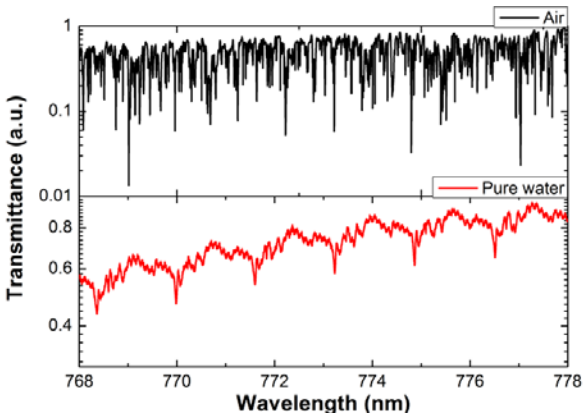

Fig. 8: Transmittance spectrum of packaged cavity in microfluidic channel in air and liquid environments.

References

[1] D. K. Armani, *et al.*, Nature **421**, 925-928 (2003).

[2] T. J. Kippenberg, PhD. Thesis (2004).

[3] Y. Yan, *et al.*, Opt. Express **19**, 5753-5759 (2011).

[4] F. Monifi *et al.*, IEEE Photonics Technol. Lett. **25**, 1458-1461 (2013).

pH measurement using a silica toroid microcavity

Jiro Nishimura (M2)　Misako Kobayashi (B4)

In this study, we measured pH using a silica toroid microcavity. An ordinary silica toroid microcavity has no sensitivity to pH, but bilayers of polyelectrolyte on a silica toroid microcavity provide pH sensitivity and we evaluated the performance.

Key words: Silica toroid microcavity; Sensing; pH; ESA

1. Introduction

Cavities have been used to improve measurement sensitivity. The effects produced by cavities are stronger when they have a higher Q-factor, which indicates the signal confinement time in a cavity, and a smaller V, which indicates signal confinement volume. Optical microcavities have attracted attention because of their high Q-factor despite their small mode volume V and they are applied to sensing [1-3]. There are various detection targets including temperature [1], proteins [2] and solution concentration [3] but pH detection alone has not been reported.

In this work, we studied an optical fiber with bilayers of polyelectrolyte [4], deposited bilayers on a silica toroid microcavity and detected pH.

2. Deposition of bilayers

It is well known that the shrinkage of a bilayer of polyelectrolyte depends on the condition of the polyelectrolyte ion [5]. The ion condition can be controlled by controlling the pH, so the bilayer thickness changes depending on the pH. Bilayers of polyelectrolyte are easily deposited by electrostatic self-assembly (ESA) and we deposited bilayers of PAH and PAA. The deposition procedure is described below.

1. Clean a toroid microcavity with piranha solution for 4 minutes. Piranha solution is H_2SO_4 : H_2O_2 = 7 : 3.
2. Clean the toroid microcavity with pure water for 1 minute.
3. Dry the toroid microcavity with N_2 gas.
4. Soak the toroid microcavity in PAH solution for 4 minutes.
5. Clean the toroid microcavity with pure water for 1 minute.
6. Soak the toroid microcavity in PAA solution for 4 minutes.
7. Clean the toroid microcavity with pure water for 1 minute. (Process of 4-7 formed a bilayer)
8. Repeat steps 4-7 of the process and form 20 bilayers on the toroid microcavity.
9. Heat the toroid microcavity with a hot plate at 60 °C for 2 hours.

Although the surface of an ordinary silica toroid microcavity has a neutral charge, it becomes negative as a result of steps 1-3 above. In this condition, soaking a toroid microcavity in PAH, which becomes a cation in solution and PAA, which becomes anion in solution, provides bilayers because of Coulomb force. Bilayer deposition realized by Coulomb force is called ESA. We purchased PAH and PAA solutions from SIGMA-ALDRICH and diluted them with pure water to 3.3 mM PAH and 2.4 mM PAA. Figure 1(a) and (b) show photographs taken before deposition, after cleaning with piranha solution and after the deposition of 20 bilayers. The Q-factor fell from 10^7 to 10^6 with the 20 bilayer deposition. Figure 1(c) shows a photograph taken after 20 bilayer deposition with 4.8 mM PAH and 6.6 mM PAA. As can be seen, too many bilayers were deposited and the Q-factor could not be measured.

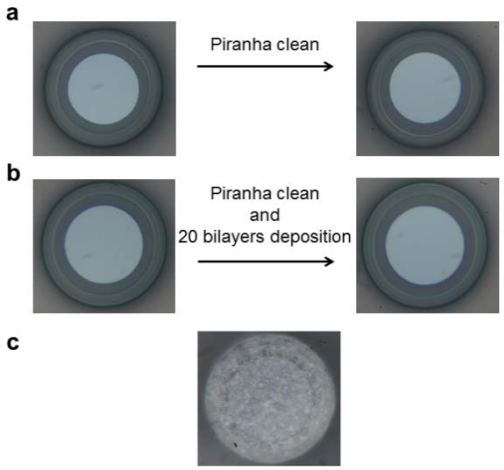

Fig. 1: Photographs of a silica toroid microcavity. (a)Before and after piranha solution cleaning. (b) Before and after 20 bilayers deposition. (c) After 20 bilayers deposition with high PAH and PAA concentrations.

3. Verification of pH sensitivity of bilayers

We verified the sensitivity of the bilayers on a silica toroid microcavity to pH. With an ordinary toroid microcavity, the resonant wavelength changes depending on the refractive index and with pH the resonant wavelength changes too because a change of thickness causes a change in the optical path length. So if we observe a resonant wavelength change that seems to be dependent on pH, we have to verify that it is due to a change in

pH not a change in refractive index. The verification procedure is described below.

1. Measure the transmittance spectrum of a toroid microcavity with 20 bilayers in a solution of 1 mL pure water and 0.125 mL sugar water. Measure the transmittance spectrum after adding each of the following to the solution.
2. 0.125 mL sugar water
3. 0.125 mL sugar water
4. 0.125 mL CH_3COOH aq
5. 0.125 mL KOH aq
6. 0.125 mL CH_3COOH aq
7. 0.125 mL KOH aq
8. 0.125 mL KOH aq

In steps 1-3, the pH did not change but the refractive index did, so the relationship between the refractive index and the resonant wavelength becomes linear. If a silica toroid microcavity with 20 bilayers is sensitive to pH, the linear relationship collapses in step 4. Figure 2 shows the relationship between the refractive index of the solution and the resonant wavelength of a silica toroid microcavity with 20 bilayers. The black, red and blue dots show the injection of sugar water, CH_3COOH aq and KOH aq, respectively, and the numbers near the dots correspond to the number of experimental procedures. As can be seen from Fig. 2, the pH change with the injection of CH_3COOH aq and KOH aq causes a larger or smaller resonant wavelength shift and it indicates that a silica toroid microcavity with 20 bilayers is sensitive to pH.

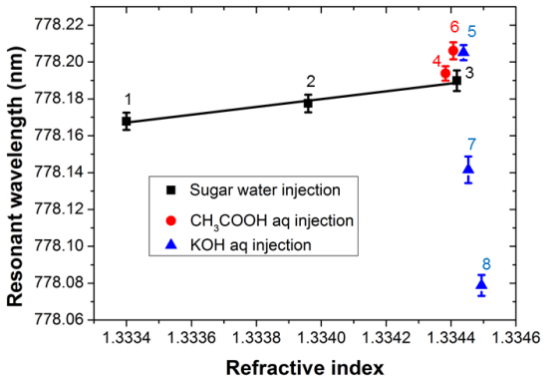

Fig. 2: Relationship between refractive index of solution and resonant wavelength of a silica toroid microcavity with 20 bilayers. Black, red and blue dots indicate the injection of sugar water, CH_3COOH aq KOH aq respectively and the numbers near dots correspond to the number of experimental procedures.

4. Neutralization titration experiment

In the previous section, we confirmed that a silica toroid microcavity with 20 bilayers is sensitive to pH and the resonant wavelength changes depending on the pH. So we detected the pH in a neutralization titration experiment. The experimental procedure is described below.

1. Measure the transmittance spectrum of a silica toroid microcavity with 20 bilayers in solution of 1 mL pure water and 0.125 mL H_2SO_4 aq.
2. Add 0.375 mL KOH aq and measure transmittance spectrum.
3. Add 0.125 mL KOH aq and measure transmittance spectrum.
4. Perform step 3 until solution becomes alkaline.
5. Add 0.125 mL H_2SO_4 aq and measure transmittance spectrum.
6. Perform step 5 until solution becomes acid.

Figure 3 shows (a) the pH of a solution measured with a commercially available pH meter and (b) the dependence of the resonant wavelength of a silica toroid microcavity with 20 bilayers on KOH aq injection until step 4 was performed. From the graphs, the results obtained with a toroid microcavity with bilayers agree well with those of a commercial pH meter, and this indicates that a silica toroid microcavity with bilayers can perform as a pH sensor. Figure 3(c) shows the relationship between pH and resonant wavelength and from the slope of the graph, we obtained a pH detection limit of 0.14.

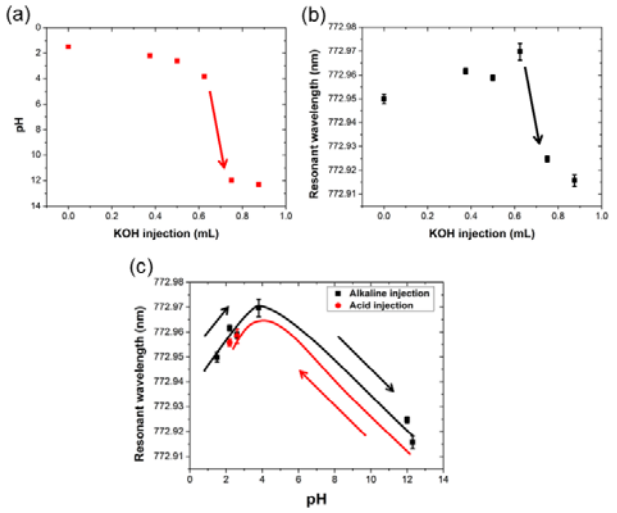

Fig. 3: (a),(b) Relationship between the injection of KOH aq and the resonant wavelength of a silica toroid microcavity with 20 bilayers. (c) Relationship between pH and resonant wavelength.

5. Conclusion

We deposited 20 bilayers of PAH and PHH on a silica toroid microcavity using the ESA technique and it showed sensitivity to pH. In a neutralization titration, the silica toroid microcavity detected a pH jump. The detection limit of this sensor is 0.14 pH and its sensitivity is not very high. However, the sensitivity is limited by laser fluctuation and so may be increased by using a high precision laser.

References

[1] A. J. Maker and A. Armani, "Heterodyned toroidal microlaser sensor," Applied Physics Letters, **103**, 123302 (2013).

[2] F. Vollmer, D. Braun and A. Libchaber, "Protein detection by optical shift of a resonant microcavity," Applied Physics Letters, **80**, 4057-4059 (2002).

[3] J. Hu, N. Carlie, L. Petit, A. Agarwal, K. Richardson and L. C. Kimerling, "Cavity-enhanced IR absorption in planar chalcogenide glass microdisk resonators: Experiment and analysis," Journal of Lightwave Technology, **27**, 5240-5245 (2009).

[4] B. Gu, M. Yin, A. P. Zhang, J. Qian and S. He, "Low-cost high-performance fiber-optic pH sensor based on thin-core fiber modal interferometer," Optics Express, **17**, 22296-22302 (2009).

[5] S. S. Shiratori and M. F. Rubner, "pH-dependent thickness behavior of sequentially adsorbed layers of weak polyelectrolytes," Macromolecules, **33**, 4213-4219 (2000).

Integration of a high-Q photonic crystal nanocavity in current silicon photonics devices

Yuta Ooka (B4), Tomohiro Tetsumoto (M2), Akihiro Fushimi (M2), Wataru Yoshiki (D1)

We report the fabrication of a high-Q photonic crystal nanocavity ($Q = 2.2\times10^5$) with photolithography. Photolithography has been used with the CMOS process and can be employed to mass-produce devices. Therefore, we can employ the existing process to fabricate photonic crystal nanocavities. Moreover, the process has high productivity. Another feature of our device is that it has SiO_2 cladding, which is also realized with the CMOS process. We show two advantageous features of the photonic crystal nanocavity. The first is that it has 4.2 times the ability to diffuse heat compared with air-bridge devices because of the silica over-cladding. The second is that it can be used for all-optical switching. The switching speed of ~0.12 ns is almost as fast as that of a previously reported photonic crystal nanoacavity fabricated with EB lithography.

Key words: Silicon photonics, photonic crystal, CMOS process, width-modulated line defect photonic crystal nanocavity, thermo-optical effect, carrier-plasma effect and all-optical switching.

1. Introduction

Silicon photonics is a candidate for the next generation of signal processing. This is because silicon, which has a high refractive index ($n = 3.47$), can both confine and propagate light with low loss in the communication band (1550 nm). Many devices have already been realized with the aim of achieving signal processing optically rather than electrically. Switches[1,2], detectors[3,4] and lasers[5,6] have been realized. These are driven by interactions between light and matter, and from that perspective confining light in a small region is important. Specifically, photonic crystal (PhC) nanocavities have been utilized due to their high Q factor and small mode volume. However, they were all fabricated with electron-beam (EB) lithography, which takes time. Moreover, they cannot be mass-produced, and their cost is high, making them impractical for usual producers. They have another disadvantage, namely an air-bridge structure. To enhance light confinement, air is chosen as the material surrounding the silicon. The structure is therefore often unstable, weak against dust and less compatible with other CMOS devices.

This report summarizes the work we undertook in the academic year 2014 to provide a solution for the two above-mentioned problems. We have confidence in the result and it will lead to the future integration of PhC nanocavities and CMOS devices.

2. Design of nanocavity

To fabricate a PhC nanocavity with photolithography properly, the design should be carefully considered. This is because the resolution with photolithography is poorer than with EB lithography and the nanocavity structure may not form as it should. We have used a PhC nanocavity design called a width-modulated line defect cavity[7]. This design is categorized as a mode-gap confinement cavity, and there is another type of design categorized as a bandgap cavity. The characteristic of the former is that it confines light in a small region using the difference between the propagation frequencies of each region along a PhC waveguide. The characteristic of the latter is that it confines light creating a relatively large structural defect in the PhC periodical structure. In addition to a width-modulated line defect cavity, we fabricated an L3 cavity[8], which is a bandgap cavity. Therefore, here we compare these two types of PhC nanocavity designs in Fig. 1. SEM images of a width-modulated line defect cavity and an L3 cavity are shown in Fig. 1(a) and (b), respectively. Although the design of a width-modulated line defect cavity will be described in detail later, the maximum shift in the hole position is 9 nm. This is seven times smaller than that of the L3 cavity (63 nm). The shift amount is very effective as regards forming the cavity structure (see Fig. 1). Two neighboring holes at the edge of an L3 cavity are connected or distorted because the proximity effect in photolithography is severe when the patterns on the photomask become too close. Considering the proximity effect in photolithography, we have concluded that mode-gap type nanocavities, which can form with a small amount of shift in the hole position, should be selected as a PhC nanocavity design for realizing robustness against photolithographic fabrication error.

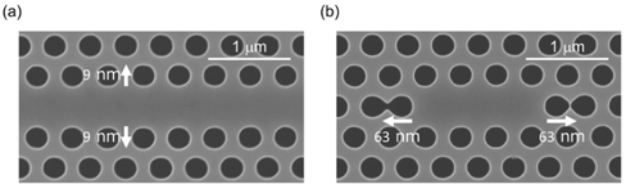

Fig. 1. SEM images of (a) a width-modulated line defect cavity and (b) an L3 cavity. The distance in each figure shows the maximum amount of shift in each cavity structure.

3. Calculation and fabrication

As discussed in the previous section, we chose a width-modulated line defect cavity for our photolithographically fabricated nanocavity. To analyze its mode profile and band structure, we performed a 3D finite-difference time domain (FDTD) and fully vectorial 3D calculation. The results are shown in Fig. 2. The

results of the 3D FDTD estimated slab thickness, hole shift and refractive indexes of Si and SiO_2 were 204 nm, 2, 4, 6 nm, 3.47 and 1.44, respectively. The calculated Q value is 7.2×10^6, which is very high despite this structure having SiO_2 cladding. The mode volume, V, is 1.7 (λ/n). And from the band diagram (Fig. 2(b)), we can see that mode-gap confinement is realized and that the wavevector is far from the light line[9], which proves that the loss in the vertical direction of the Si slab is suppressed.

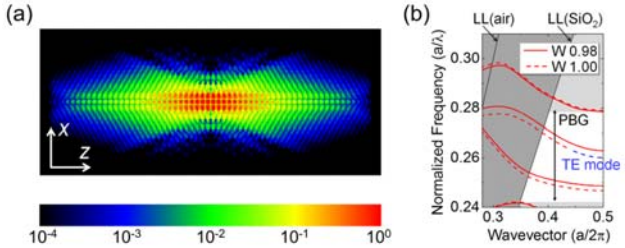

Fig. 2. (a) Mode profile of H_z component calculated by 3D FDTD simulation. (b) Band diagram of the structure. The red and red dashed lines show the bands of a PhCWG whose widths are W0.98 (mirror), W1.00 (cavity), respectively.

We employed the services of the Institute of Microelectronics (IME), Singapore, which uses a CMOS compatible photolithographic process. In this process, an ArF (excimer laser of 248 nm) is used for the exposure. They decided the slab thickness of 210 nm, so the actual design we used corresponds to the schematic shown in Fig. 3.

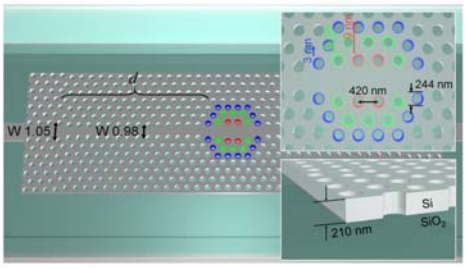

Fig. 3: Schematic of a PhC nanocavity fabricated with a photolithographic CMOS process.

4. Fundamental characteristics

Utilizing the design and process described above, we fabricated a width-modulated line defect cavity with SiO_2 cladding and measured certain characteristics. In this section, we discuss the transmittance, Q-factor and thermal diffusion ability.

The transmittance of the fabricated device is shown in Fig. 4. The measuring light is coupled to a Si nanowire via a spot size converter (SSC), which takes advantage of the use of the photolithographic CMOS process. Because of this the coupling loss is only 0.8 dB. The inset shows the expansion of the cavity mode peak whose center wavelength is around 1619.20 nm. This is in the photonic bandgap of the W0.98 region, which can be explained by the steep band edge seen around 1615 nm. Lorentzian fitting is applied to the peak, which exhibits a Q factor of 2.2×10^5. This value is the highest for a photolithographic PhC nanocavity.

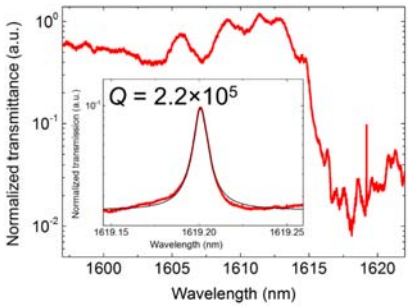

Fig. 4. Transmittance of a PhC nanocavity with a Q of 2.2×10^5. The inset shows the expansion of the peak region and the black line is a calculated Lorentzian fitting.

Next, another measurement was conducted in which the input light wavelength was scanned four times with various input powers. When the intra cavity power increases and the thermo-optical (TO) effect appears relatively strong, optical bistability is observed (see Fig. 5). In this measurement, we used a SiO_2-clad cavity with a Q of 2.1×10^5, and the threshold power was 19 μW. This value is four times that of the air-bridge structure with almost the same Q (2.3×10^5). This result shows that SiO_2 cladding has an advantage in terms of heat diffusion. This is very useful when it is applied to signal processing architecture, because heat (in the cavity region) usually causes a pattern effect due to its slow diffusion time.

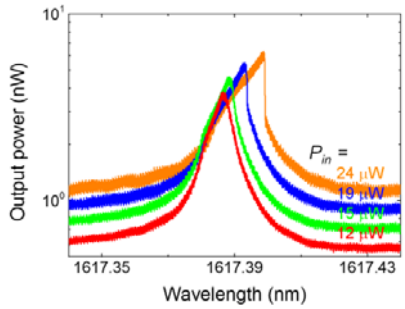

Fig. 5. Resonant wavelength shift toward red side due to TO effect. The threshold when optical bistability is observed is 19 μW (intra cavity power).

5. All-optical switching

Finally we performed all-optical switching with the device we described in previous sections. The switching speed is defined in several ways, and here it is defined as the time at which the light power becomes half the maximum contrast to the time at which it recovers. The Q factor corresponds to the ability to confine light, and thus light will be trapped for a long time in a high-Q nanocavity. This is undesirable because a faster driving speed is necessary for switching. Therefore, a device with a Q of 3.6×10^4 (one order lower than the device with the highest Q) was selected in this demonstration.

The result provided in Fig. 6(a) was obtained with the setup shown in Fig. 6(b). Here, the switching technique was the control-signal method[2]. This is the first demonstration of all-optical switching with photolithographic PhC nanocavities. The switching speed is 0.12 ns and this value is the same as that of a previous report in which a PhC nanocavity fabricated with EB lithography was used[2].

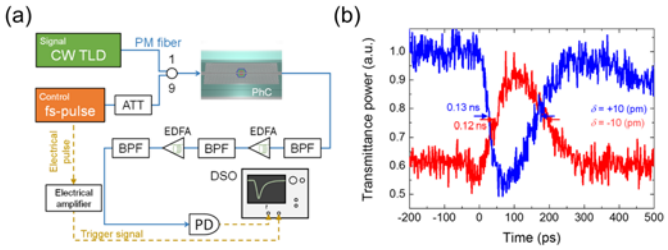

Fig. 6. All-optical switching. (a) Schematic of setup. (b) Modulated transmittance in time domain.

6. Conclusion

We realized a PhC nanocavity fabricated with a photolithographic process that has a high Q and SiO_2 cladding. This is the first time that all-optical switching with photolithographic PhCs has been demonstrated, and the switching speed is the same as that of previous EB lithographic PhCs. This work will lead to the integration of PhC nanocavities and CMOS devices.

References

1. Almeida, V. R., Barrios, C. A., Panepucci, R. R. & Lipson, M. All-optical control of light on a silicon chip. *Nature* **431,** 1081–1084 (2004).
2. Tanabe, T., Notomi, M., Mitsugi, S., Shinya, A. & Kuramochi, E. All-optical switches on a silicon chip realized using photonic crystal nanocavities. *Appl. Phys. Lett.* **87,** 151112 (2005).
3. Yin, T. *et al.* 31GHz Ge n-i-p waveguide photodetectors on Silicon-on-Insulator substrate. *Opt. Express* **15,** 13965–13971 (2007).
4. Tanabe, T., Sumikura, H., Taniyama, H., Shinya, A. & Notomi, M. All-silicon sub-Gb/s telecom detector with low dark current and high quantum efficiency on chip. *Appl. Phys. Lett.* **96,** 101103 (2010).
5. Rong, H., Liu, A., Jones, R., Cohen, O. & Hak, D. An all-silicon Raman laser. *Nature* **433,** 292–294 (2005).
6. Takahashi, Y. *et al.* A micrometre-scale Raman silicon laser with a microwatt threshold. *Nature* **498,** 470–474 (2013).
7. Kuramochi, E. *et al.* Ultrahigh-Q photonic crystal nanocavities realized by the local width modulation of a line defect. *Appl. Phys. Lett.* **88,** 041112 (2006).
8. Akahane, Y., Asano, T. & Song, B. High- Q photonic nanocavity in a two-dimensional photonic crystal. *Nature* **425,** 4–7 (2003).
9. Srinivasan, K. & Painter, O. Momentum space design of high-Q photonic crystal optical cavities. *Opt. Express* **10,** 670 (2002).

Large thermo-optic effects in silica-gold composite toroidal microcavity

Sho Tamaki (M1)

We experimentally demonstrated an optical switch using the thermo-optic effect with extremely low power and a large resonant wavelength shift using a silica-gold composite toroidal microcavity. We employed a sputtering method to fabricate the silica-gold composite cavity.

Key words: Thermo-optic effect; Gold nanoparticle; Silica toroidal microcavity

1. Introduction

Optical microcavities are being closely studied since they may pave the way to a large reduction in the energy consumed in optical telecommunication. Among the many different types of optical microcavities, the silica toroidal microcavity is widely known for its high quality factor (Q) and small mode volume (V). When using this device as an optical switch, the thermo-optic (TO) effect is a candidate as its operating principle since the size of the effect is easily modulated by controlling the input power. However, it should be noted that this operating principle normally requires a power of over 1 mW [1-3]. In this study, we show a large enhancement in the thermo-optic effect through observing the resonant wavelength shift and optical switching achieved at extremely low power by doping a silica toroidal microcavity with gold. It is also widely known that silica-gold composite material has a greater Kerr effect than silica alone thanks to its surface plasmon resonance. We will show the greater Kerr effect in our cavity in future work.

2. Resonant wavelength shift by TO effect

2.1 Fabrication and Evaluation

To fabricate a silica-gold composite microcavity, we first fabricated a silica disk cavity using photolithography, silica etching and XeF_2 etching. We then sputtered a gold layer approximately 3.2 nm thick onto the silica disk cavity and irradiated a CO_2 laser from above.

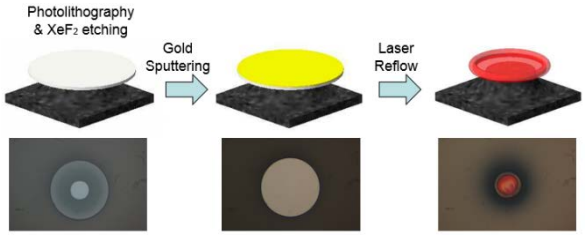

Fig. 1: Fabrication of silica-gold composite microcavity. The cavity in the picture is one example. (No experimental results are provided in this paper.)

Before performing optical switching, we compared the resonant wavelength shift of the cavities with and without gold as shown in Fig. 2. We obtained Q factors of 5×10^5 and 3.3×10^6 for the cavities with and without gold, respectively. As shown in Fig. 2, the cavity with gold exhibits a large resonant wavelength shift despite the Q factor being lower than that of the cavity without gold.

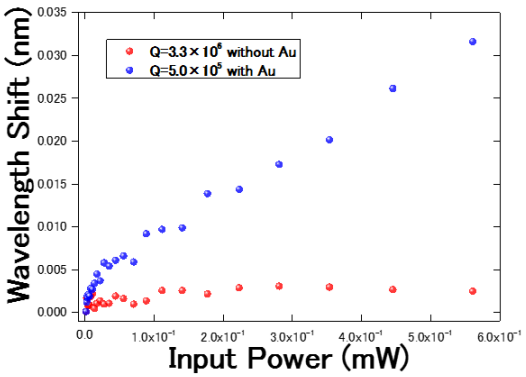

Fig. 2: Relationship between input power and resonant wavelength shift of cavities with and without gold.

2.2 Analysis and Discussion

Having acquired the resonant wavelength shift with different input powers, we estimated the Q factor limited by the material absorption using COMSOL to calculate the heat capacity of the cavity. Eventually, we obtained the Q factor limited by the material absorption of 3.4×10^6.

3. Optical switching using TO effect

3.1 Experimental results

Figure 3 shows our experimental setup.

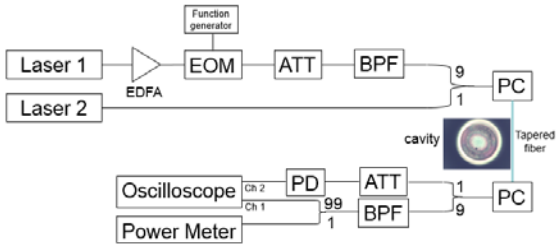

Fig. 3: Experimental setup for optical switching using TO effect.

Before performing the TO optical switching, we obtained two different cavity modes, namely the control and signal modes. For the control mode, we obtained $\lambda = 1542$ nm and a loaded Q factor of 8×10^5. For the signal mode, we obtained $\lambda = 1572$ nm and a loaded Q factor of 9×10^5.

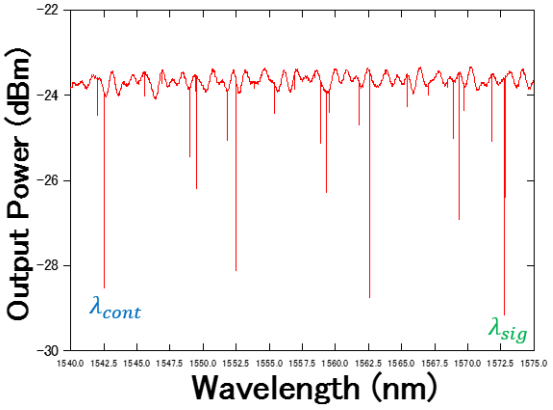

Fig. 4: Transmission spectrum of cavity.

Figure 5 shows the results of TO effect optical switching with different input powers. The control pulse light width was set at 6 ms. The signal cooling time was approximately 1.5 ms regardless of the input power. Eventually, we performed optical switching with a minimum input power of 12.5 μW using the TO effect. We believe that this is the lowest power operation yet reported for optical switching using the TO effect.

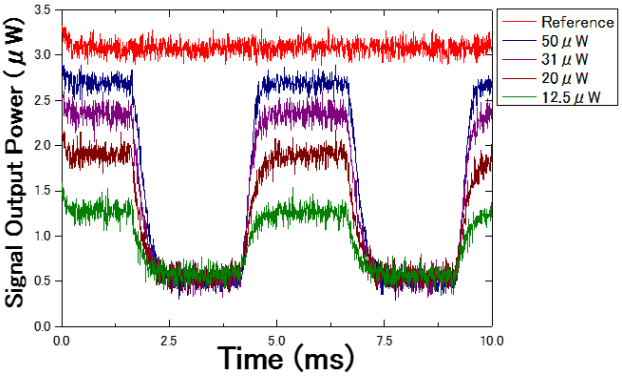

Fig. 3: Thermal optical switching operation with different input powers.

3.2 Discussion

To show how small a power this is, in Table 1 we summarize the TO optical switching performance reported in previous studies. As shown, our device operates at a much lower power than other devices. This enhancement results from doping the silica toroidal microcavity with gold, as well as maintaining a high Q factor.

Table 1. TO Optical Switching Performance

Device	Response Time	Power
Fabry-Perot [1]	0.62 μs	58.4 mW
Waveguide [2]	14 μs	6.5 mW
Silica Toroid [3]	80 μs	1.9 mW
This work	1.5 ms	12.5 μW

4. Conclusion

We demonstrated an enhanced resonant wavelength shift and the extremely low power operation of optical switching by fabricating a silica-gold composite toroidal microcavity. This kind of composite material based cavity will pave the way for the development of optical microcavities.

References

[1] Marcel W. Pruessner, Todd H. Stievater, Mike S. Ferraro, and William S. Rabinovich "Thermo-optic tuning and switching in SOI waveguide Fabry-Perot microcavities," Opt. Exp. **15**, 7557-7563 (2007).

[2] Adam Densmore, Siegfried Janz, Rubin Ma, Jens H. Schmid, Dan-Xia Xu, Andre Delage, Jean Lapointe, Martin Vachon and Pavel Cheben, "Compact and low power thermo-optic switch using folded silicon waveguides " Opt. Exp. **17**, 10457-10465, (2009).

[3] Wataru Yoshiki and Takasumi Tanabe, "All-optical switching using Kerr effect in a silica toroid microcavity," Opt. Exp. **22**, 24332-24341, (2014).

Design of a MOMS switch based on a zipper cavity

Tomohiro Tetsumoto (M2)

We demonstrate numerically the feasibility of a radiation pressure driven micro opto-mechanical system (MOMS) directional switch based on a silica zipper cavity. The silica zipper cavity has an optical Q of 4.0×10^4 and a mode volume of $2.1(\lambda/n)^3$. We also show that an extinction ratio of over 17.8 dB can be obtained with an input power of 190 mW.

Key words: Cavity opto-mechanics; Optical radiation pressure; Zipper cavity; optical switch;

1. Introduction

The improvement in the performance of optical cavities enables us to enhance the optical radiation pressure effectively. This has opened a new research field called cavity opto-mechanics, which involves the study of devices driven with optical force [1]. In this work, we propose the new concept of a micro-opto-mechanical-systems (MOMS) switch and demonstrate numerically the feasibility of a directional switch driven with optical radiation pressure.

The operating principal of the proposed optical switch is shown schematically in Fig. 1. The switch is based on a directional coupler composed of two evanescently coupled waveguides. The energy exchanges between the two waveguides during signal propagation. The direction of the signal light is determined by the coupling length and the gap distance between the waveguides (coupling strength). Our idea is to change the gap distance and modulate the coupling strength using optical radiation force; and thus change the route of the output light all-optically. We used a suspended directional coupler that can move horizontally. We also formed a zipper cavity [2] in the center of the directional coupler to enhance the optical radiation force. We chose to use silica for our device to minimize the propagation loss of the telecom signal light.

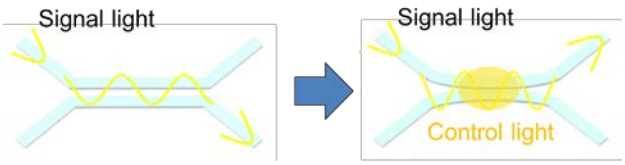

Fig. 1: Operating principle of proposed optical switch

2. Optical and mechanical design of zipper cavity

We first designed a zipper cavity and analyzed the optical properties of the cavity with 3D FDTD. The zipper cavity amplifies the intensity of a control light. We adopted the design parameters of the cavity as shown in Fig. 2(a) and set the resonant wavelength in the visible range. The mode profile of the cavity is shown in Fig. 2(b). Fig. 2(c) shows the gap dependence versus quality factor and mode volume. The highest Q/V was obtained when the gap was 34 nm. The values are a Q of 4.0×10^4 and a V of $2.1(\lambda/n)^3$.

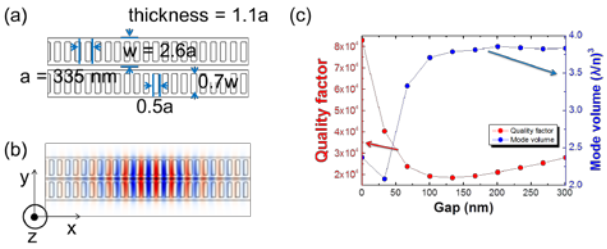

Fig. 2: (a) Design of zipper cavity. (b) Ey mode profile. (c) Gap dependence versus Q and V.

Next, we analyzed the mechanical properties of the zipper cavity using the finite element method (FEM) with COMSOL Multiphysics 4. 3. Representative oscillation modes are shown in Fig. 3. The horizontal mode is dominant in this study because the optical force acts horizontally. We set the length of the device at 41.2 μm and obtained a mechanical eigen frequency of 3.2 MHz. We also obtained an oscillation decay time of $\tau = \Omega_m/Q_m = 3.1$ μs assuming that the mechanical quality factor in air is about 10. This decay time is almost the same as the operating time of the device.

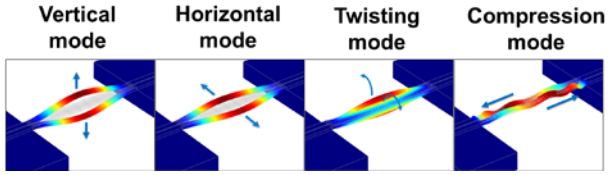

Fig. 3: Representative oscillation modes of zipper cavity

3. Analysis of light propagation

We analyzed the light propagation in the device with 2D FDTD. The computing model is shown in Fig. 4(a). We placed a light source at the upper left of the waveguide and monitored the time average of the energy transmittance at sampling points in

the upper right and lower right of the waveguide. We then calculated the extinction ratio using the following equation.

$$\text{(Extinction ratio)} = \left|10 \log\left(\frac{E_2}{E_1}\right)\right| \quad (1)$$

The computation results are shown in Fig. 4(b). We obtained an extinction ratio of 17.8 dB when the gap was 193 nm, which was the initial state. When we reduced the gap to 92 nm, we obtained an extinction ratio of 18.2 dB. This shows that we can obtain a switching contrast of over 17.8 dB with a 100-nm deformation.

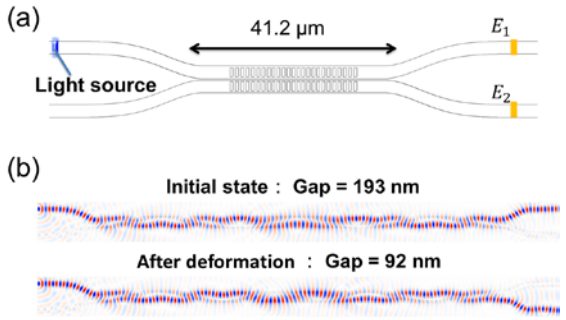

Fig. 4: (a) Computing model of light propagation. (b) Result of light propagation computation.

4. Optical and mechanical coupling

Finally, we analyzed the power required to deform the structure by 100 nm. Assuming an adiabatic process, we can describe the radiation force F as $F = dU/ds = \hbar\, d\omega/ds$ where U is the energy in the cavity and ds is the minute distance change of the gap. We analyzed the gap dependence versus resonant wavelength and show the result in Fig. 5(a). The calculated optical force and opto-mechanical coupling ratio g_{OM} (= $d\omega/ds$), which indicates the strength of opto-mechanical coupling, are shown in Fig. 5(b). We can see that the designed cavity has a high opto-mechanical coupling ratio of over 100 GHz/nm.

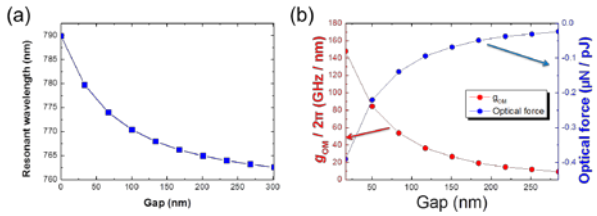

Fig. 5: (a) Gap dependence versus resonant wavelength. (b) Gap dependence versus g_{OM} and optical force.

We then calculated the deformation caused by the optical radiation force using FEM. Assuming the complete coupling of the control light, we can describe the energy in the cavity as $U = QP_{in}/\omega$ where P_{in} is the input power of the control light. We estimated the boundary area S in which the optical force acts from the mode volume of the cavity and the slot gap s as $S = V/s$. We applied a boundary load to the structure and finally found that an input power of 190 mW is sufficient to deform the structure by 100 nm.

Although we have finished the entire device design process, we still have to consider the regenerative amplification threshold. If the opto-mechanical gain exceeds the mechanical damping, the oscillation of the structure will be amplified to be divergent and the device will not work well. The effective damping of the device is described by the following equation [1],

$$\Gamma_m' = \Gamma_m - \left(\frac{2U g_{OM}^2 \Gamma}{\omega_0 m_{eff}}\right) \frac{\Delta}{\left(\Delta^2 + \left(\frac{\Gamma}{2}\right)^2\right)^2} \quad (2)$$

where Γ_m is the fundamental mechanical damping, Γ is the optical damping rate, ω is the optical resonant angular frequency, and Δ is the detuning from the resonant frequency. The input power and detuning dependence versus effective mechanical damping is shown in Fig. 6. The input power line at 200 mW is well above the regenerative threshold over the entire range. So we need have no concern about regenerative amplification in this study.

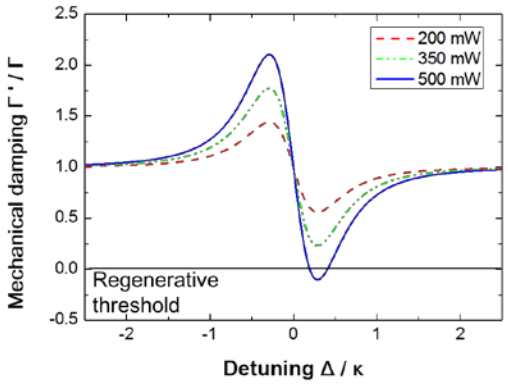

Fig. 6: Input power dependence versus effective mechanical damping.

5. Summary

In this study, we described a numerical study of an opto-mechanical directional switch. The designed cavity has a high quality factor of 4×10^4 and a small mode volume of $2.1(\lambda/n)^3$. We obtained a high extinction ratio of over 17.8 dB with an input power of 190 mW. The operating speed of the device is 3.1 μs. The details of the study are summarized in our article [3]. Future work will include the fabrication of the structure and experimental analyses.

References

[1] T. J. Kippenberg and K. J. Vahala, Opt. Express **15** 17173 (2007).
[2] M. Eichenfield, *et al.*, Nature **459** 550 (2009).
[3] T. Tetsumoto and T. Tanabe, AIP Advances **4** 077137 (2014).

Fabrication of CaF_2 microcavity and observation of thermo-opto-mechanical oscillation

Hiroki Itobe (B4)　Yosuke Nakagawa (M1)

We can realize a continuous pulse light source that is both inexpensive and compact, by achieving a wider bandwidth and the stabilization of an optical Kerr comb in a CaF_2 microcavity. In this work, we established a process for fabricating microcavities using ultra-precision cutting that allows us to control the bandwidth of the optical Kerr comb. We demonstrated experimentally the necessity of reducing thermo-opto-mechanical oscillation to stabilize the optical Kerr comb.

Key words: Whispering-gallery-mode microcavity; CaF_2; Optical Kerr comb

1. Introduction

A whispering-gallery-mode (WGM) microcavity is an element in which light circulates and is trapped in a micro-volume. The efficiency with which light is trapped in the microcavity is called the Q value and this is ultimately restricted by the material absorption property of the microcavity. Calcium fluoride (CaF_2) has a very low absorption coefficient in the communication wavelength band, so it may enable us to make a microcavity that has a very high Q value ($Q > 10^9$). Previous research reported the fabrication of a $Q = 6.3 \times 10^{10}$ microcavity.

2. Wider bandwidth and stabilization of optical Kerr comb

An optical Kerr comb is a non-linear optical effect observed in WGM microcavities. An optical Kerr comb is an equal interval spectrum in the frequency domain, and a continuous pulse light source in the time domain. An optical frequency comb can be observed by using a mode-locked laser, which is similar to an optical Kerr comb. The advantages of the optical Kerr comb are that the WGM microcavity is cheaper and smaller, and the disadvantages are that it is difficult to achieve a wider bandwidth and stabilization. On the other hand, the advantages of the optical frequency comb are that a wider bandwidth and stabilization can be realized easily, and the disadvantages are that a mode-locked laser is larger and more expensive. Hence, we will achieve a wider bandwidth and stabilization of the optical Kerr comb, and a cheaper and smaller continuous pulse light source by employing a WGM microcavity.

To realize an optical Kerr comb with a wider bandwidth, it is necessary to bring the distribution value close to zero in a wide frequency domain. The distribution value consists of a material distribution value and a structure distribution value. The former is determined by the CaF_2 property and cannot be controlled, whereas the latter can be controlled by designing the cross sectional shape of the microcavity. With the previous method, it is necessary to polish the microcavity surface to obtain sufficient smoothness and a satisfactory Q value. However, this process deforms the cross sectional shape, which also alters the structure distribution value. Therefore, we adopted an ultra-precision cutting process to make the microcavities, which enables us to cut CaF_2 bulk precisely and keep the bulk surface smooth. We can simultaneously achieve a high Q value and control the structure distribution value.

To stabilize the optical Kerr comb, we must reduce the thermo-opto-mechanical (TOM) oscillation. The oscillation is caused by two effects; a thermo-optical effect, which shifts the cavity resonance toward a shorter wavelength, and thermal expansion, which shifts the cavity resonance toward a longer wavelength. Thus the resonance wavelength goes back and forth around the input wavelength and the intracavity power fluctuates periodically. This disturbs stable optical Kerr comb generation, so it is necessary to reduce the TOM oscillation.

3. Fabrication of CaF_2 microcavity with ultra-precision cutting

Fig. 1 shows a CaF_2 microcavity fabricated with ultra-precision cutting. The cutting was undertaken by the Kakinuma Laboratory, which is part of our university. The microcavity has a diameter of 500 μm, a surface roughness of about 3 nm, and a Q of 3.0×10^6. We also polished the microcavity and

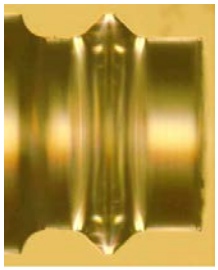

Fig. 1 Photograph of fabricated CaF_2 microcavity.

to give it a surface roughness of about 3 nm, which is almost the same as before polishing, and a Q of 1.2×10^7, which is higher than before polishing. Detailed research shows that ultra-precision cutting forms a polycrystalline layer on the surface of the microcavity, whose thickness is about 50 nm. This layer has higher absorption properties than a monocrystalline bulk, and this may lead to a lower Q value.

4. Thermo-opto-mechanical (TOM) oscillation

The Q value is measured by sweeping an input wavelength from shorter to longer. We changed the input optical power from 1 mW to 1 W, which strengthens the nonlinear optical effect that occurs in a microcavity, and observed that the optical power oscillates periodically. When we inverted the sweep direction, no oscillation was observed. Fig. 2 shows these results.

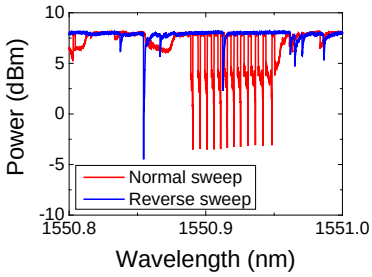

Fig. 2 Spectrum corresponding to two wavelength sweep directions.

The oscillation is caused by a shift in the resonance wavelength of the microcavity caused by a thermo-optical effect and thermal expansion. It is shown by Eq. 1.

$$\lambda_r(t) = \lambda_0 \left(1 + \frac{dn}{dT_1} \Delta T_1(t) + \alpha \Delta T_2(t) \right) \quad (1)$$

$\lambda_r(t)$ is the resonance wavelength, λ_0 is the steady resonance wavelength, dn/dT_1 is the thermo-optical coefficient, α is the thermal expansion coefficient, $\Delta T_1(t)$, $\Delta T_2(t)$ are the temperature changes from the steady state of the mode volume and the entire microcavity volume. Unlike silica (Si) and silicon (SiO_2), which have positive thermo-optical coefficients, CaF_2 has a negative thermo-optical coefficient and the sign of its thermal expansion coefficient is opposite to that of CaF_2. These effects balance and resonances occur repeatedly, which results in the observation of TOM oscillation. Fig. 3 shows these results.

(a)

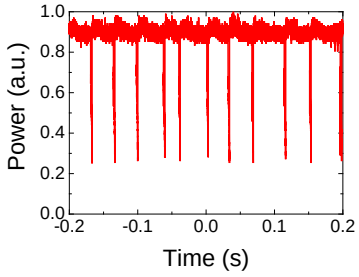

(b)

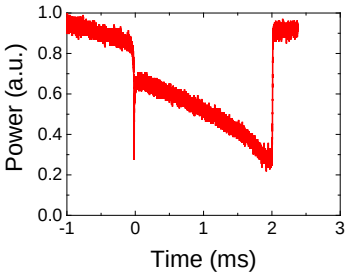

(c)

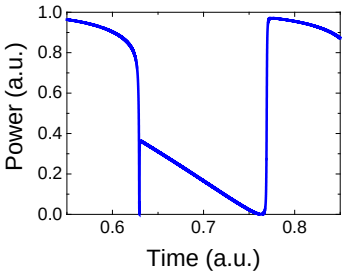

Fig. 3 (a) TOM oscillation (input wavelength is locked).
(b) magnifying (a).
(c) Simulation result based on Eq. 1.

It is important for the TOM oscillation that the thermo-optical effect and the thermal expansion are well balanced, and the rates depend on the ratio of the mode volume and the entire microcavity volume. A shorter wavelength shift takes a relatively short time and a longer wavelength shift takes a relatively long time. Fig. 2 shows that an oscillation occurs only when the input wavelength is swept from shorter to longer. This can be explained by the fact that the longer wavelength shift remains for a long time compared with the shorter wavelength shift. Moreover, the larger a microcavity is, the longer it takes for heat to conduct in the microcavity, so we assumed that the heat in the microcavity saturates before the TOM oscillation occurs. To confirm this hypothesis, we fabricated a microcavity with a diameter of about 6 mm (see Fig. 4(a)), and carried out the same experiment. As a result, no oscillation was observed (see Fig. 4(b)).

(a)

(b)

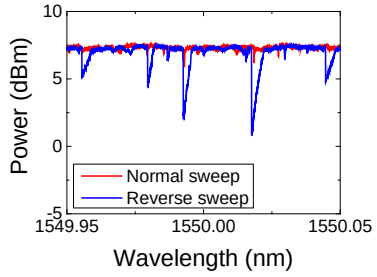

Fig. 4 (a) Microcavity with 6 mm diameter.

(b) No oscillation was observed.

5. Relation between TOM oscillation and optical Kerr comb

An optical Kerr comb occurs only when the intracavity optical power is above a threshold optical power. Thus, with CaF_2 microcavities, the intracavity optical power fluctuates due to TOM oscillation, so the optical Kerr comb appears and disappears repeatedly. In fact, there are cases where the optical Kerr comb is observed (see Fig. 5(a)), and cases where it is not observed (see Fig. 5(b)).

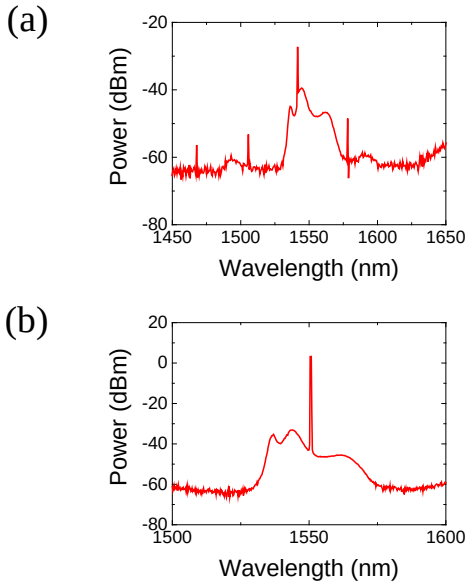

Fig. 5 (a) Optical Kerr comb is observed.
(b) Optical Kerr comb is not observed.

To demonstrate the repeated appearance of the optical Kerr comb, we carried out an experiment where an input wavelength (1540-1560 nm) passes through a low pass filter (1540-1564 nm) and a high pass filter (1570-1610 nm). When the optical power through the high pass filter changes, it implies that an optical Kerr comb is detected. The result is shown in Fig. 6(a), (b). It means that the optical Kerr comb is unstable because of the influence of the TOM oscillation.

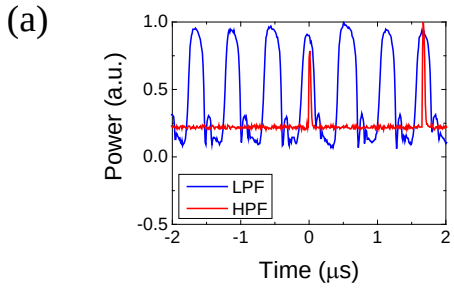

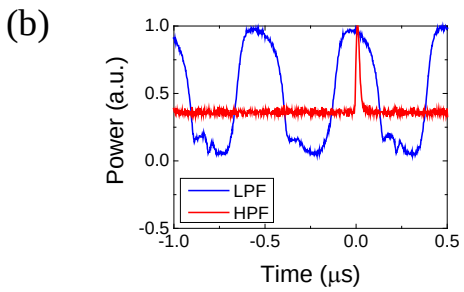

Fig. 6 (a) Optical Kerr comb is detected.
(b) enlarged view of (a).

6. Conclusion

We established a process for fabricating CaF_2 microcavities very precisely with ultra-precision cutting. The microcavities have a diameter of 500 μm and a surface roughness of 3 nm. A microcavity has a Q value of 3.0×10^6, which is smaller than the polished value. This problem may be solved by removing the polycrystalline layer from the surface of the microcavity. In the future, it will be necessary to design an ideal cross sectional shape for a microcavity to realize an optical Kerr comb with a wider bandwidth.

Detailed research showed how a TOM oscillation occurs, and the importance of the ratio between the mode volume and the entire microcavity volume. The optical Kerr comb becomes unstable due to the TOM oscillation, and we must find a way to reduce it. An effectiveness of enlarging the microcavity size is shown experimentally. However, it also reduces the intensity of the non-linear optical effect. Therefore, we have to find the optimum microcavity size using a numerical study or a good structure with effective heat conduction, to stabilize the optical Kerr comb.

References

[1] A. A. Savchenkov, V. S. Ilchenko, A. B. Matsko, and L. Maleki, "Kilohertz optical resonances in dielectric crystal cavities", Phys. Rev. A **70**, 051804(R) (2004).

[2] B A. I. Rahachou and I. V. Zozoulenko, "Effects of boundary roughness on a Q factor of whispering-gallery-mode lasing microdisk cavities", J. Appl. Phys. **94**, 7929 (2003).

[3] G. Lin, S. Diallo, R. Henriet, M. Jacquot, and Y. K. Chembo, "Barium fluoride whispering-gallery-mode disk-resonator with one billion quality-factor", Opt. Lett. Vol. **39**, No. 20 (2014).

[4] L. He, Y.-F. Xiao, J. Zhu, S. K. Ozdemir, and L. Yang, "Oscillatory thermal dynamics in high-Q PDMS-coated silica toroidal microresonators", Opt. Express **17**, 9571 (2009).

[5] M. J. Weber, "*Handbook of Optical Materials*", (CRC Press, 2002), Vol. **19**

Statistical Data

Publications (Apr. 2014 – Mar. 2015)

Journal papers

[1] W. Yoshiki and T. Tanabe, "Performance of Kerr bistable memory in silicon nitride microring and silica microtoroid," Jpn. J. Appl. Phys. Vol. 53, No. 12, 12202 (pp. 7) (2014).

[2] W. Yoshiki and T. Tanabe, "All-optical switching using Kerr effect in a silica toroid microcavity," Opt. Express, Vol. 22, No. 20, pp. 24332-24341 (2014).

[3] A. Fushimi, H. Taniyama, E. Kuramochi, M. Notomi, and T. Tanabe, "Fast calculation of the quality factor for two-dimensional photonic crystal slab nanocavities," Opt. Express, Vol. 22, No. 19, pp. 23349-23359 (2014).

[4] S. Azami, K. Hiroshi, T. Tanabe, J. Yan, and Y. Kakinuma, "Experimental analysis of the surface integrity of single-crystal calcium fluoride caused by ultra-precision turning," Procedica CIRP, Vol. 13, pp. 225-229 (2014).

[5] T. Tetsumoto and T. Tanabe,"High-Q silica zipper cavity for optical radiation pressure driven MOMS switch," AIP Advances, Vol. 4, 077137 (2014).

[6] A. Fushimi and T. Tanabe, "All-optical logic gate operating with single wavelength," Opt. Express, Vol. 22, No. 4, pp. 4466-4479 (2014).

International conferences

[1] R. Saito, M. Terakawa, and T. Tanabe, "Optical spectrum measurement of a cell-adhered microcavity for the cell-cycle analysis applications," APS March Meeting 2015, H1.00045, San Antonio, March 2-6 (2015).

[2] Z. Chen, W. Yoshiki, and T. Tanabe, "Broad-bandwidth pulse transmission through an ultrahigh-Q nanocavity with a chirped pulse," 2014 Frontiers in Optics/Laser Science Conference (FiO/LS), FTu5D.6, Tucson, October 19-23 (2014).

[3] T. Tetsumoto and T. Tanabe, "High-Q silica zipper cavity with strong opto-mechanical coupling for optical radiation pressure driven directional switching," IEEE Photonics Conference 2014 (IPC2014), San Diego, October 12-16 (2014).

[4] A. Fushimi, H. Taniyama, E. Kuramochi, M. Notomi, and T. Tanabe, "Fast and accurate calculation of Q factor of 2D photonic crystal cavity," CLEO:2014, JTh2A.49, San Jose, June 6-13 (2014).

[5] A. Fushimi and T. Tanabe, "Robustness of scalable all-optical logic gates," JTu4A.93, CLEO:2014, SM1M.7, San Jose, June 6-13 (2014).

[6] T. Kato, R. Suzuki, T. Kobatake, and T. Tanabe, "Analysis and experiments on harmonic mode locking in an optical microcavity," CLEO:2014, SM1M.7, San Jose, June 6-13 (2014).

[7] R. Suzuki, T. Kato, T. Kobatake, and T. Tanabe, "RF noise measurement of a

microcavity Kerr comb generated by dual pumping," The 3rd Advances Lasers and Photon Sources (ALPS' 14), ALPS3-5, Yokohama, April 22-25 (2014).

Dissertations

Master thesis:

Ryusuke Saito, “Optical spectrum measurement of a cell-adhered microcavity for the cell-cycle analysis applications”

Tomohiro Tetsumoto, “Study on an all-optical switch based on a silica zipper cavity operating with optical radiation pressure”

Jiro Nishimura, “Study on detection of ions and pH in liquid using a silica toroid microcavity”

Akihiro Fushimi, “Study on the construction of logic gates with small optical cavities”

Bachelor thesis:

Hiroki Itobe, “Study on the measurement of optical nonlinear effect using crystalline whispering gallery mode cavity”

Yuta Ooka, “High Q photonic crystal nanocavity fabricated with CMOS process”

Yusuke Okabe, “Noise analysis and feedback control for the stabilization of the frequency of optical Kerr comb in a microcavity”

Misako Kobayashi, “Study on Fixing technology of a tapered optical fiber with a silica toroid microcavity and application for sensing”

Takuma Nagano, “Study on mode-locking of optical Kerr comb by time domain measurement”